


## Article

# Wetland Fire Assessment and Monitoring in the Paraná River Delta, Using Radar and Optical Data for Burnt Area Mapping

Héctor Del Valle <sup>1</sup>, Walter Fabián Sione <sup>1,2</sup>  and Pablo Gilberto Aceñolaza <sup>1,3,4,\*</sup>

- <sup>1</sup> Centro Regional de Geomática (CeReGeo), Facultad de Ciencia y Tecnología, Universidad Autónoma de Entre Ríos (UADER), Ruta 11 km 10.5, Oro Verde 3100, Entre Ríos, Argentina
- <sup>2</sup> Departamento de Ciencias Básicas, Universidad Nacional de Luján (UNLu), Luján 6700, Buenos Aires, Argentina
- <sup>3</sup> Centro de Investigaciones Científicas y Transferencia de Tecnología a la Producción (CICYTTP-CONICET), España 149, Diamante 3105, Entre Ríos, Argentina
- <sup>4</sup> Facultad de Ciencias Agropecuarias, Universidad Nacional de Entre Ríos (FCA-UNER), Ruta 11 km 10.5, Oro Verde 3100, Entre Ríos, Argentina
- \* Correspondence: acenolaza@gmail.com

**Abstract:** In the past decades, important research has been carried out to map the natural disturbances in the Paraná River Delta. The benefits of the combined use optical and radar data are also known. The main objective of this paper is to assess the wetland fire cartography through a synergetic use of radar and optical data. We focus on integrating radar (SAOCOM) and Sentinel 1, as well as Sentinel 2 optical data, concerning the fires impact analyses in the wetland areas. The generation of water masks through the radar images can contribute to improve the burned wetland area estimations. The relationship between landforms, vegetation cover, and the spatial/temporal resolution imposed by the flood pulse, play a vital role in the results. Burnt areas represent a total of 2439.57 sq km, which is more than 85% of the wetland, during the winter and spring (Q3 and Q4) periods. Understanding the wetland heterogeneity and its recovery pattern after a fire, is crucial to improve the cartography of the burned areas; for this, biweekly or monthly image compositions periodicity are of crucial importance. The inclusion of different indexes, for optical and radar images, improve the precision for the final classification. The results obtained here are promising for post-flood and post-fire evaluation, even applying radar and optical data integration into the evaluation and the monitoring of wetland fires is far from being a uniform standardized process.

**Keywords:** l-band; optical and radar indices; wetland burnt area maps; wetland fires



**Citation:** Del Valle, H.; Sione, W.F.; Aceñolaza, P.G. Wetland Fire Assessment and Monitoring in the Paraná River Delta, Using Radar and Optical Data for Burnt Area Mapping. *Fire* **2022**, *5*, 190. <https://doi.org/10.3390/fire5060190>

Academic Editors: Keith T. Weber and Grant Williamson

Received: 30 August 2022

Accepted: 7 November 2022

Published: 12 November 2022

**Publisher's Note:** MDPI stays neutral with regard to jurisdictional claims in published maps and institutional affiliations.



**Copyright:** © 2022 by the authors. Licensee MDPI, Basel, Switzerland. This article is an open access article distributed under the terms and conditions of the Creative Commons Attribution (CC BY) license (<https://creativecommons.org/licenses/by/4.0/>).

## 1. Introduction

Land degradation (LD) processes have socio-ecological components at multiple scales in space and time [1–3]. The interactions between scales are sometimes complex and occur when socio-ecological components interact between scales. When undetected, such interactions can cause errors in the extrapolation data from one region to another. In general, the challenges of acquiring data at broad spatial extents, lead to the cross-scale interactions not being systematically investigated [4,5].

Argentina is a country that needs to establish operational digital land degradation mapping (LDM) initiatives to address challenges and solutions at detailed and semi-detailed scale levels [6]. These efforts could provide useful environmental information to complement or update existing LD data and document methods and results.

In the last decades, algorithm refinements of optical and radar archives, have led to progressively improved research-quality products, ideally suited for studies of land use, mapping, and monitoring [7].

The Group on Earth Observations (GEO) is a unique partnership consisting of national governments and international organizations aimed at ensuring that the information about

our planet, is available to all ([http://earthobservations.org/geo\\_ldn.php](http://earthobservations.org/geo_ldn.php), access date: 1 November 2021). Earth observation data cubes (EODC) have emerged as a promising solution to efficiently and effectively handle big Earth observation data (BEOD), generated by satellites and made them freely and openly available from different data repositories [8]. It is also important to highlight the potential of open-source software and the importance of the inter-linkages between these and remote sensing training, with an interdisciplinary perspective [9–11].

During the past 50 years, an unprecedented expansion of land degradation has affected soil resources. Among them, fires strongly disturb environmental features, such as the ecosystem services, by increasing soil erosion [12–17]. Due to land use intensification, the above mentioned pattern, is also present in the Paraná River subbasin [14,15]; this intensification produce soil erosion which affects the land quality and water resources [16].

Moreover, the Paraná River Delta is affected by two major stressors, the flood pulse [17,18] and the fire regime [18–20]. Burning grassland is a historic land management practice in this wetland, associated with cattle ranching [21]. In this heterogeneous wetland, more than 80% of the vegetation is herbaceous and highly diverse, while only 4% is occupied by native forests and a similar area is occupied by forest plantations [22]. This landscape has suffered recurrent fire episodes in recent decades, especially in 2008 and 2012, with dense smokes that affected a large region in Central Argentina [23,24]. At the present time, a prolonged period of unusually warm weather and drought in the upper basin (Southern Brazil, Paraguay, and Northern Argentina) has dropped the Paraná River's water levels to its lowest in decades [25]. Lower water levels imply more area, mostly grassland and shrubs, available to be burnt. In 2020, the fires burned 3290 sq km and were out of control [26].

In this context, the main objectives of this paper were to assess and monitoring LD through a synergetic use of radar and optical data. Our specific objectives were to better understand the spatial and temporal LD patterns (specifically wetland fires) and to evaluate the different remote sensing data for near real-time degradation monitoring.

## 2. Materials and Methods

### 2.1. Study Area

The study area is the distal portion of the Paraná River (delta area) which is the third-largest river in the American continent, after the Mississippi in the United States and the Amazonas in Brazil. (Figure 1).

The Paraná River Delta is the largest wetland in Argentina and spreads along the final 330 km of the Paraná basin, from south of Diamante city (32°03'52" S; 60°38'33" W) to the vicinity of Buenos Aires city (34°36'47" S; 58°22'38" W). It comprises 17,500 sq km, it is a floodplain with numerous islands with changing shapes and areas, according to the variable dynamics of the water level (fluvial/tidal) and the short- and long-term evolution of the river [22,27]. Through the Paraná Delta and the Rio de la Plata estuary, the river drains into the Atlantic Ocean, from the second major hydrographic basin of South America (La Plata Basin).

Major threats are related to climate variability (flood and drought phases), and human impacts [15,19,20,28,29]. A direct relationship was found between the climatological droughts, low water levels on the Paraná River, and the increased fire activity within the delta [20]. Lower water levels mean more area, mostly grassland, is available to be burnt [30]. At the present time, the economic development of the Delta is focused on transforming wetlands into terrestrial ecosystems, by creating a water management infrastructure; these environmental changes are aimed at building urban recreational areas, cattle grazing, forestry, and agricultural areas [15,31,32].

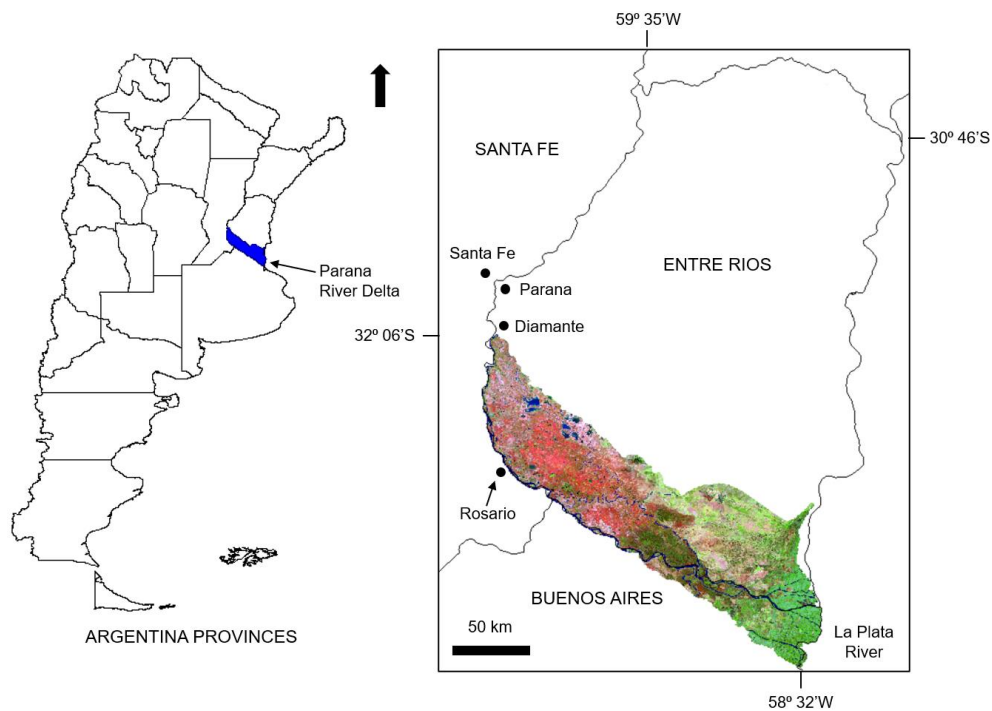


**Figure 1.** Location of the Paraná River Delta. S2 mosaics from October 2020, RGB 12-8-4. Note the soil moisture differences between burned areas (red colors) and their unaffected surroundings (green colors).

2.2. Data Sources and Collection

Table 1 summarizes the input (reference) datasets used in this study and the image preprocessing for microwave and optical remote sensing.

**Table 1.** Sources of the remote sensing data.

Data	Satellite/Other Sources	Date	Spatial Resolution m	Data Source
L-band, TNQP images		- 10 March 2020 - 4, 9 and 25 October 2020	50	
L-band, SQP images	SAOCOM-1A	- 5 July 2020 - 20 August 2020 - 18 September 2020 - 9 October 2020	10	CONAE
C-band, GRDH, SDV images	SENTINEL-1A/B	- 31 October 2018 - 1, 6 and 11 January 2020 - 3 and 4 June 2020 - 21 and 28 July 2020 - 2, 3, 26 and 27 August 2020 - 19 and 20 September 2020 - 25, 26, and 31 October 2020	10	ESA
Mosaic: Blue, Green, Red, NIR, SWIRS, and SWIRL bands	SENTINEL-2	2018 Quarters 2020 - January to December 2020 - January 2021	10, 60	SENTINEL-2 Global Mosaic Consortium (S2GM)

TNQP: TOPSAR narrow quad polarization. SQP: StripMap quad polarization. SAOCOM: Satélite Argentino de Observación Con Microondas, Spanish for Argentine Microwaves Observation Satellite. CONAE: National Space Activities Commission, Argentina. GRDH: Ground Range Detected High resolution. SDV: SAR standard dual VV/VH. ESA: European Space Agency.

### 2.2.1. SAOCOM-1A Data

The Argentine Satellite of Observation with Microwaves (SAOCOM) is a constellation of two Earth observation satellites owned by the Argentinean National Commission for Space Activities (CONAE). Both satellites present a L-band synthetic aperture radar (SAR) and were launched in October 2018 (SAO1A) and August 2020 (SAO1B).

To allow the acquisition times close to the time of environmental emergencies, on the one hand, and to obtain enough data, on the other hand, SAO1A data had to be collected in different orbits and angles of incidence. We use the StripMap (SM) and TOPSAR narrow (TN) modes available in the ascending and descending right hand viewing, respectively, and quad polarization ( $L_{HH}$ ,  $L_{HV}$ ,  $L_{VH}$ , and  $L_{VV}$ ). The minimum incidence angle range was  $23.2^{\circ}$ – $25.4^{\circ}$  and  $17.6^{\circ}$ – $27.3^{\circ}$  for SM and TN, respectively. The Geocoded Ellipsoid Corrected images (GEC) were chosen as they can be easily imported into geographic information systems (GIS). This format consists of radiometrically geocoded data, concerning a reference ellipsoid [33]. The product's 1C level is in absolute values (amplitude). The backscatter is given as sigma-naught ( $\sigma^0$ ).

### 2.2.2. SENTINEL-1 Data

SENTINEL-1 (S1) operates at 5.405 GHz, with a radar wavelength of 5.6 cm (C-band) and provides four exclusive imaging modes with different resolutions and coverage. Special attention was paid to the StripMap (SM), interferometric wide swath (IW), Ground Range Detected High resolution (GRDH) products. Free open access (S1 A/B) data are available through the Copernicus Open Access Hub (<https://scihub.copernicus.eu>, accessed on 15 December 2020). The satellite data were acquired by sensors S1A and S1B, with right hand viewing, descending pass, in  $C_{VV}$  and  $C_{VH}$  with an incident angle of  $30.6^{\circ}$ – $46.3^{\circ}$ .

### 2.2.3. SENTINEL-2 Global Mosaic

The SENTINEL-2 Global Mosaic (S2GM) service (sentinel-hub.com), offers mosaic surface reflectance products derived from the S2 A/B platforms. Input to the processing is the Level 2A (L2A) products, provided by the Copernicus Ground Segment [34]. We use this service to generate temporal composite periods (month, quarter, year) at the mesoscale (60 m and 20 m) and microscale levels (10 m) with a high confidence cloudless sky over the study areas. The bands included were B2 (blue), B3 (green), B4 (red), B8 (near-infrared, NIR), B11 (Short-Wave Infrared Short reflectance, SWIRS), and B12 (Short-Wave Infrared Long reflectance, SWIRL).

## 2.3. Workflow

The data methodological processing for the Paraná River Delta study area, is illustrated in the Figure 2.

The following open-source software packages were used for the digital processing: QGIS 3.16.2 [35], System for Automated Geoscientific Analyses (SAGA GIS) v7.9.0 [36], SAS Planet v180518.9750 Nightly [37], Sentinel Application Platform (SNAP) v8.0 [38], Google Earth Pro v7.3.3.7786 [39], and R statistic packages v3.5.0 [40].

### 2.3.1. Optical Vegetation Indices

In this study, the vegetation indices derived from S2 were used. The vegetation radiometric indices selected were the normalized difference vegetation index (NDVI), normalized difference water index (NDWI), normalized burn ratio (NBR), and the normalized burn ratio 2 (NBR 2).

We selected the NBR and NBR 2, as they have been widely used in previous burn area mapping algorithms [41–44] and NDVI, as it was successfully used in the area [20,23]. As water bodies can show a similar NBR difference in certain circumstances, it is necessary to mask them. The S2 products are cloud-free, so there was no need to remove the clouds. For this purpose, a single water mask was generated. Thus, the normalized difference water index (NDWI) was used to detect water surface and its spatial and temporal dynamics.



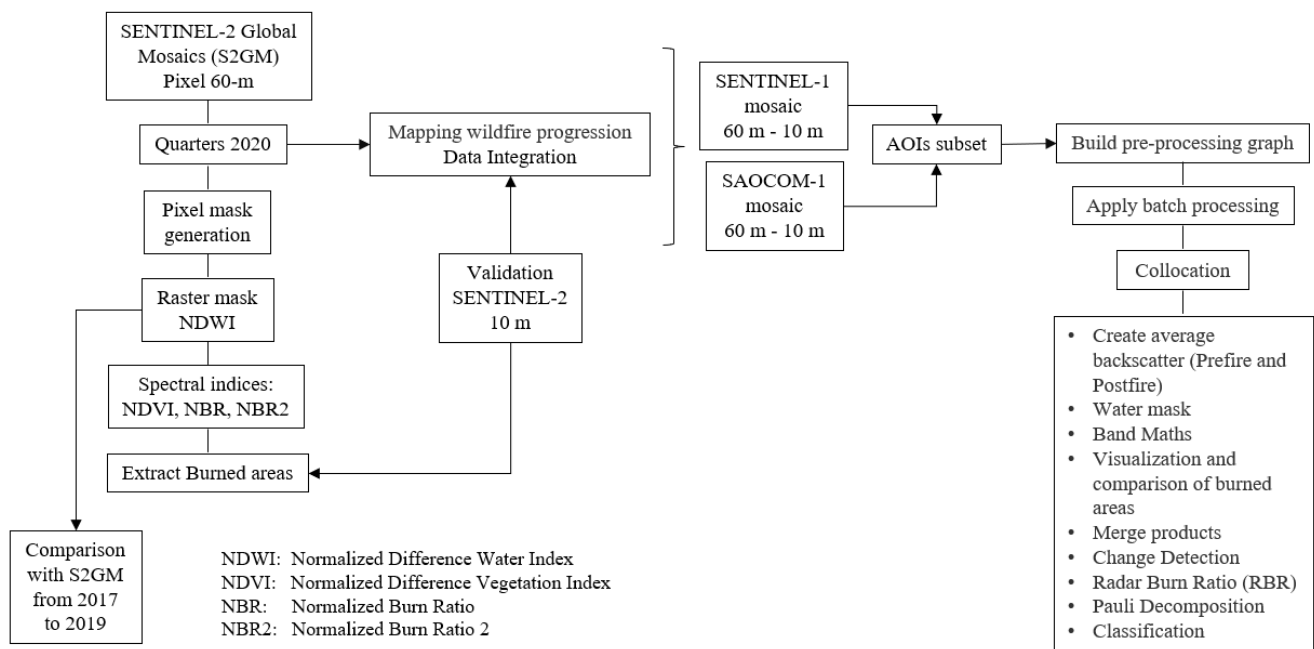


**Figure 2.** Workflow analysis for the burned area mapping in the Paraná River Delta.

### 2.3.2. Optical and Radar Integration

The “Collocation” Tool, in the SNAP software, allows the placement of spatially overlapping products. This algorithm involves the pixel values of a slave product (optical data) that are resampled into the geographical raster of a master product (SAR data). Thus, a new product was created which contains a copy of all of the components of the master and slave products. This is a key step for the image integration as it allows for a range of different methods, to utilize the information content of both products (visual interpretation, histogram and statistics, band math, mask manager, working with vectors, and classification).

### 2.3.3. Feature Extraction and Classification

The burnt area mapping was carried out using S2 and S1 datasets, independently, and all pixels detected as burnt, were combined into a mapped composite. Following the pre-processing, the vegetation indices were calculated using the S2 bands, and the results were included in the integration data set. Given the limited availability of the SAO1A images, they were only used for two areas of interest (AOIs).

We studied the capability of different S2 mosaics (2017–2020) to estimate the water cover or water presence–absence [45]. The water mask was calculated using the NDWI index.

The S2 baseline burned areas were generated from quarterly and monthly 2020 mosaics. Although the first fires started in February (Q1), the focus was on quarters 3 and 4 (Q3 and Q4). The time length between the quarterly observations was limited to avoid confusion, due to the changes in landcover not related to fire, or due to misinterpretation of a fire signal over areas with rapid vegetation growth (herbaceous vegetation). The latter is a feature of the Paraná River Delta fires [20,23]; for this reason, monthly areas of interest (pixel 10-m) were considered (from July 2020 to January 2021), where the progression of fires and the recovery of herbaceous vegetation, could be observed.

The separability index (SI), also called the normalized distance, was used to evaluate the performance of spectral indices (NDVI, NBR, and NBR 2), in terms of their capability for the discrimination of burned and unburned areas [46]. It is computed as follows:

$$M = [ub - \mu_{ub}] / (\delta_{ub} + \delta_{ub})$$

where  $\mu_b$ : mean values of the considered spectral band of the burned area;  $\mu_{ub}$ : the mean values of the considered spectral band of the unburned area;  $\delta_b$ : the standard deviations of spectral values of the burned area;  $\delta_{ub}$ : the standard deviations of spectral values of the unburned area. For the computation of the separability index, we used the Zonal statistics tool in R statistic packages v3.5.0 [40]. With this tool, the mean and standard deviation values of the burned and unburned areas were obtained using the reference burned/unburned images (S2 mosaic pixel 10-m). Higher separability index values indicate that the given spectral index has a strong separability attribute, whereas lower values reflect that the discrimination of the burned and unburned pixels are not as good as the higher SI values.

The thresholds for the spectral indices were determined, based on the visual inspection of fire scars. We optimize these thresholds to accurately represent the burned area, minimizing false positive detections in the neighboring unburned areas.

The data processing for the identification and mapping of burned areas with radar data, was carried out without using fixed threshold values [47,48]. According to various authors, fire produces contrasting effects on the behavior of backscattering [49,50]. Combustion reduces and/or increases scattering from the ground, due to a diminished signal attenuation and increased effects of surface conditions and soil properties [51,52]. We use the improved expectation–maximization (EM) algorithm and the Bayesian inferencing applied to the change detection algorithm. The classification of the burned area was based on an iterative process of visual inspection, delineation of the training polygons, and classification.

The radar burn ratio (RBR) involved the computation of post-fire (Quarter 3, 2020) to pre-fire (Quarter 1, 2020) ratio of the backscattering coefficients in decibel (dB) units:

$$RBR_{xy} = \text{Post-fire average backscatter}_{xy} / \text{Pre-fire average backscatter}_{xy}$$

$RBR_{xy}$  was calculated for each polarization (i.e., VV and VH).

This index was used as a measure of fire severity and change of backscatter [44].

Both S1 and SAO1 backscatter coefficients were used to identify the anomalous changes in the radar signal and to associate them with biomass burning [53,54]. The temporal resolution may vary between seven days to one month, depending on the SAR availability and the actual acquisition frequency. We consider multi-temporal changes of the backscatter intensities, together with the optical information on the burned areas.

#### 2.3.4. Accuracy Assessment

Two areas of interest (AOIs) were created to place, randomly, 200 circular ground points, each with a 120 m diameter. These points were used to validate both burnt area mosaics obtained by optical and radar image analyses.

The burnt area products were obtained by applying a fixed threshold to the normalized burned ratio S2 (NBR 2 difference) in Sentinel 2; the other product was the burned area classification with S1 (BAC S1), both obtained in an initial 60-m resolution burned/not burned cartography. These products were visually evaluated, in each of the 200 ground points, using monthly S2 images (10 m resolution).

The Kappa statistics, along with the total accuracy of the classified AOIs, were performed to measure the extent of classification accuracy.

### 3. Results and Discussion

#### 3.1. Wetland Change Patterns: Water Surface Detection

The increasing frequency of extreme events in the La Plata basin affects the Paraná River flow [17]. Figure 3 shows the spatial and temporal changes in the water surface from S2 mosaics at a 60-m resolution (2017 to 2020).

The NDWI was used to extract the water information from the land surface. This index is closely related to the water surface and shows an asymptotic relationship in the Paraná River Delta [41]. Low NDWI values were present in the quarters from 2020 (period of water stress), corresponding to a low vegetation water content and low vegetation fraction cover.

The NDWI average were  $-0.65 \pm 0.11$  (Q1),  $-0.63 \pm 0.10$  (Q2),  $-0.47 \pm 0.10$  (Q3), and  $-0.47 \pm 0.23$  (Q4).

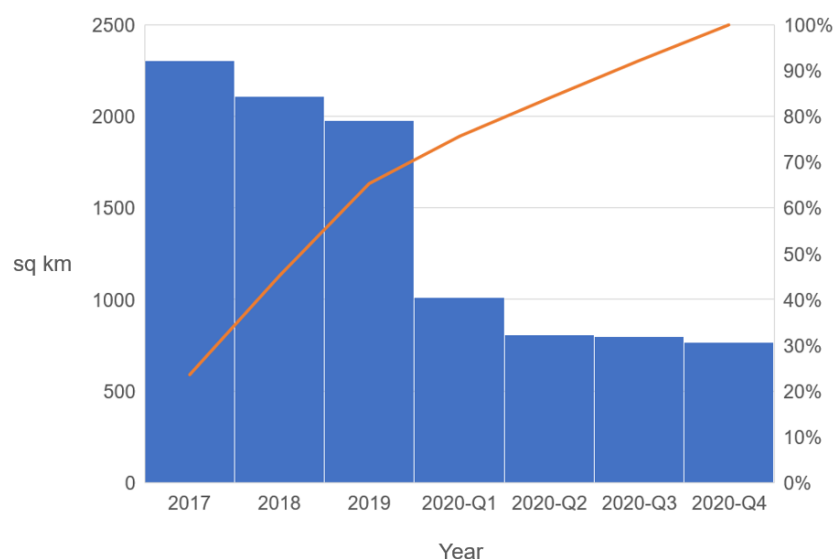


**Figure 3.** Pareto chart that contains both bars and a line graph, where individual values from the water surface, in sq km per year and quarters (2020), are represented in descending order by bars, and the cumulative total is represented by the red line.

The period studied was influenced by drought, within a prolonged period dominated by low water flows, combined with dry weather and fires [25]. The high influence of the hydrology of this large river on the Delta emphasizes the relevance of changes in its flow (pulse) regime in recent decades, such as the seasonality attenuation [55].

In general, the NDWI rate of change would suggest that the hydrology factors of the wetlands were divided into water bodies and non-aquatic bodies (that is, dry soil on the land surface) with different dynamic proportions [56].

### 3.2. Burned Area Detection and Mapping with S2

Figure 4A–D shows the quarterly (January to December 2020) S2 mosaics. The quarters demonstrate how the mosaics at 60-m pixel resolution RGB 12-8-4, provided through the S2 Global Mosaic service (S2GM) can help to track burned areas in time, depending on whether the area is cloud-free. In the detailed Figure 4B–D, the burnt areas (red colors) are visible with the fire-induced changes in the quarters (Q2, Q3, and Q4). Special attention was given in Q3 (winter), since although in July, the burned area was small, in August, the difference between the combustion and the burned area showed the most obvious change. In September, the burned area reached its maximum range during the observation period, which also coincides with the historical annual fire pattern [20,23].

Fires at the Paraná River Delta affect mainly the herbaceous vegetation and are, in general, of short duration and relatively small in size, with a seasonal pattern of occurrence usually in early spring to early summer, and are highly variable from year to year [20]. With less frequency, fire is also used during autumn and early winter [23]. The progression of fire burned areas (red colors) and the partial restoration of herbaceous vegetation (green colors) are shown in Figure 5 (10-m pixel resolution). These comparisons show that the different wetland cover locations, burned at different severities, subsequently recovered their seasonal green cover profiles to stable pre-fire levels in a very short time. This was reported by Zamboni and Aceñolaza [57], who found a recovery of the herbaceous vegetation five months after an extensive fire, with spectral response values similar to those before the fire. This behavior was explained by the main floristic composition of the wetland present with many C4 grasses.

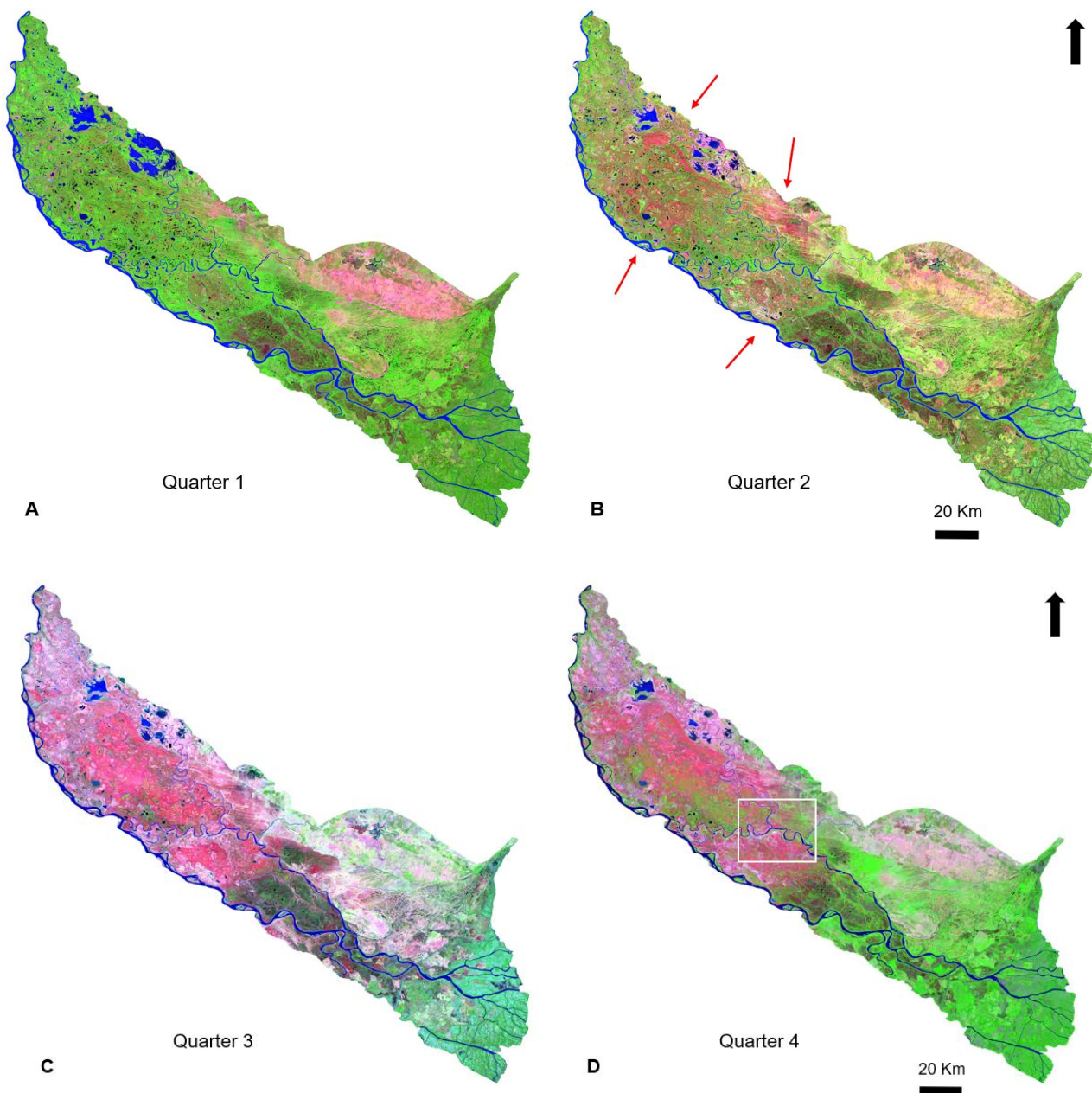


**Figure 4.** (A,B) Paraná River Delta: Wetland fire. The burnt areas (red colors) are highlighted in the S2 (RGB 12-8-4) imagery. The quarterly mosaics were freely downloaded from S2GM (sentinel-hub.com), with a high confidence clear sky. (A). Quarter 1 (January-February-March 2020). (B). Quarter 2 (April-May-June 2020). Pixel resolution 60-m. (C,D) The quarterly mosaics were freely downloaded from S2GM (sentinel-hub.com), with a high confidence clear sky. (C). Quarter 3 (July-August-September 2020). (D). Quarter 4 (October-November-December 2020). Pixel resolution 60-m. White rectangular polygon locates Figure 5.

Salvia [30] identified that, after one growing season, vegetation recovery is dependent on fire severity and the hydrological condition, while soil properties did not show signs of recovery. The ash deposition could cause the loss of substantial levels of organic matter and loose unstructured soil; it must be considered that these soils are Entisols and do not present a horizontal structuration [16]. High-severity wildfires have been shown to have long-term impacts on freshwater ecosystems; as nutrients are mobilized, the runoff and erosion can increase, and soil properties may be modified [58].



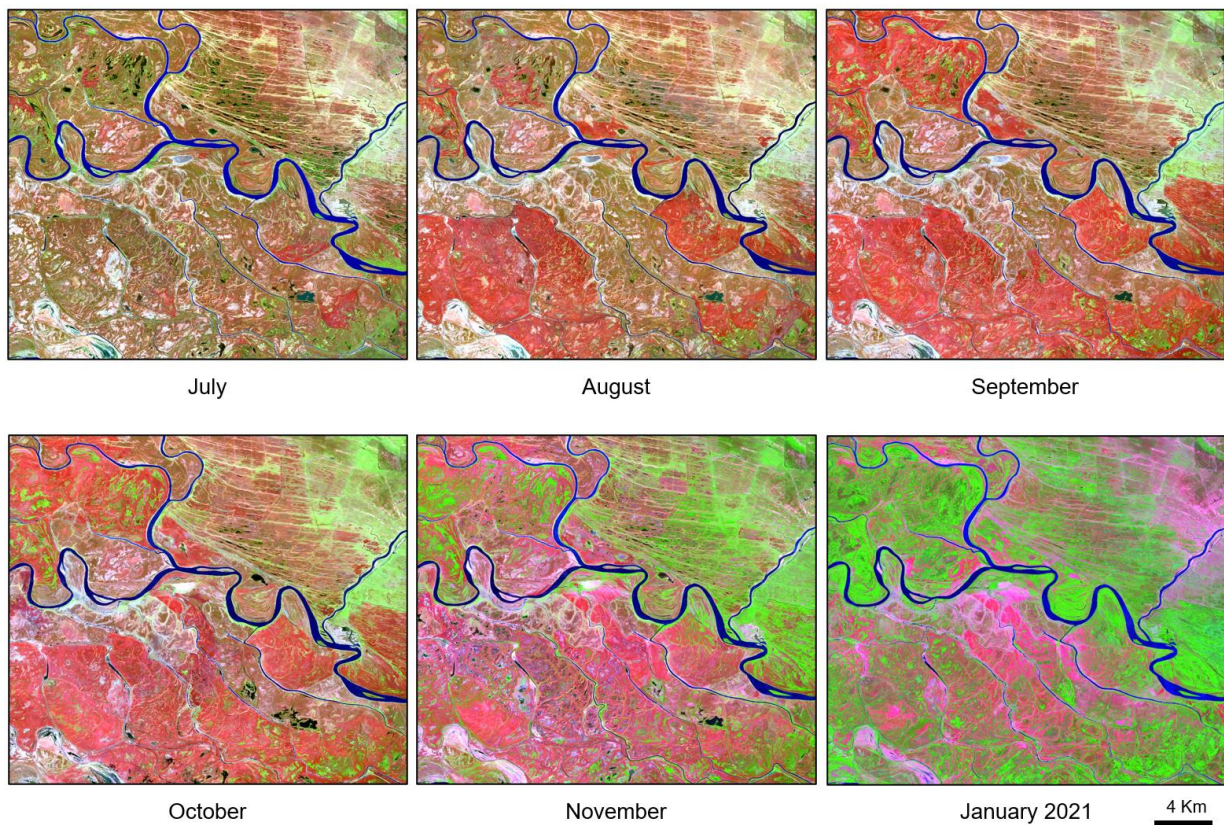


**Figure 5.** Burned areas (red colors) showing the progression of fire and the partial restoration of herbaceous vegetation (green colors). The monthly mosaics were freely downloaded from S2GM (sentinel-hub.com), with a high confidence clear sky. RGB 12-8-4. July to November 2020 and January 2021. Pixel resolution 10-m.

Among the SIs analyzed (Table 2), the NBR 2 provided the highest discriminating ability and is the only SI with values higher than one. The NBR had M-values between 0.5 and 1 and the NDVI revealed little discriminatory power. Figure 6A,B shows the results obtained from the normalized burn ratio 2 (NBR 2) for Q3 and Q4, respectively.

**Table 2.** Separability index for the spectral indices.

	NDVI	NBR	NBR 2
Mean $\mu_b$ , burned	0.23	0.14	−0.23
Mean $\mu_{ub}$ , unburned	0.10	−0.001	−0.06
Standard deviations $\delta_b$ , burned	0.15	0.11	0.09
Standard deviations $\delta_{ub}$ , unburned	0.06	0.08	0.06
M, separation index	0.62	0.74	0.93

We apply a fixed threshold of  $NBR\ 2 < -0.2$  to obtain an initial burned/not burned area which is cross-checked against the existence of the S2 mosaic at a 10-m pixel resolution. The algorithm uses consecutive S2 quarters (Q2, Q3, and Q4) to derive a burned area map at 60-m spacing (Figure 7).



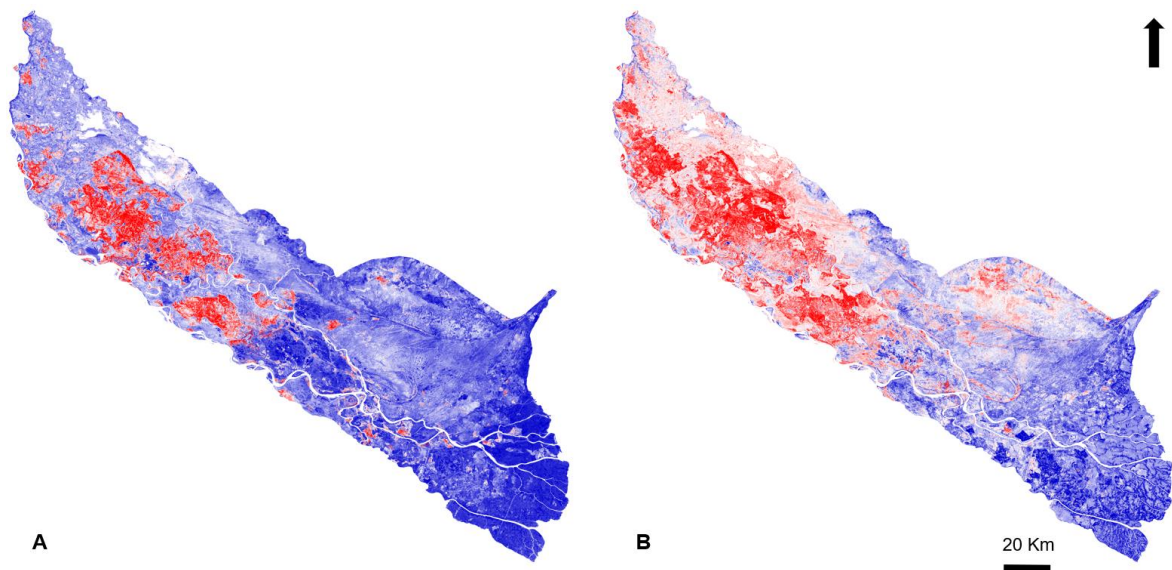


**Figure 6.** (A,B) Normalized burn ratio 2 (NBR 2). Pixel resolution 60-m. (A). Quarter 3 (June-August-September 2020). (B). Quarter 4 (October-November-December 2020).

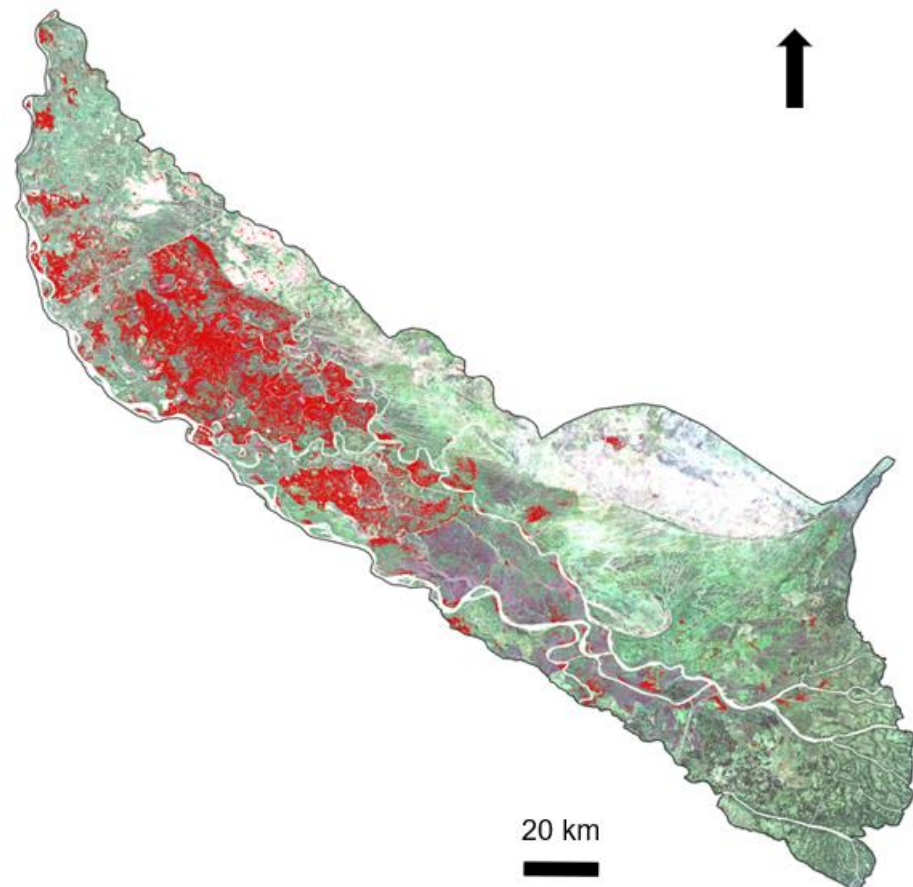


**Figure 7.** Burned areas detection and mapping in the Paraná River Delta, using S2 (April to December 2020).

The areas burned per quarter were 82.44 sq km (Q2-Q1); 2135.57 sq km (Q3-Q2); and 221.56 sq km (Q4-Q3), with a total of 2439.57 sq km.

The overall accuracy and Kappa coefficient of the extracted results of wetland fires reached 74% and 0.43, respectively (Table 3).

**Table 3.** Accuracy assessment of the Paraná River Delta classification with normalized burned ratio with S2 (NBR 2 difference).

		NBR 2 Difference		Total	Commission Errors
		Burned	Not-Burned		
S2-mosaic pixel 10-m	Burned	43	33	76	0.434
	Unburned	19	105	124	0.153
Total		62	138	200	
Omission errors		0.306	0.239		0.74

Overall accuracy: 74%. Kappa: 0.43.

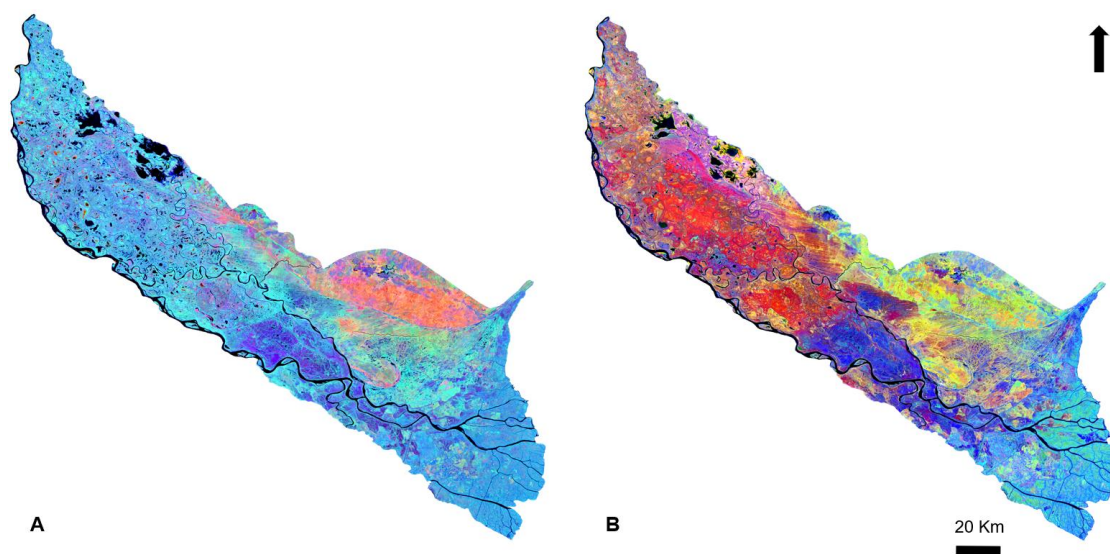
These statistics show that timing and hydrology are important driving factors. Fires radically change their ranges, as the river level variation affect the area subjected to be burned, as found by Zamboni et al. [20]. However, the change in hydrology conditions after a fire does not always decrease gradually and linearly over time.

The flooding pulses create temporal heterogeneities in the landcover [17]. During the flooding period, the soil is mostly covered by water and macrophytic plants, while during the period of low water, those areas remain covered by semi-decomposed aquatic plant debris. This material responds, spectrally, in similar fashion to charcoal, increasing the detection error of the burned areas [20,23].

### 3.3. Burned Area Detection and Mapping with S1

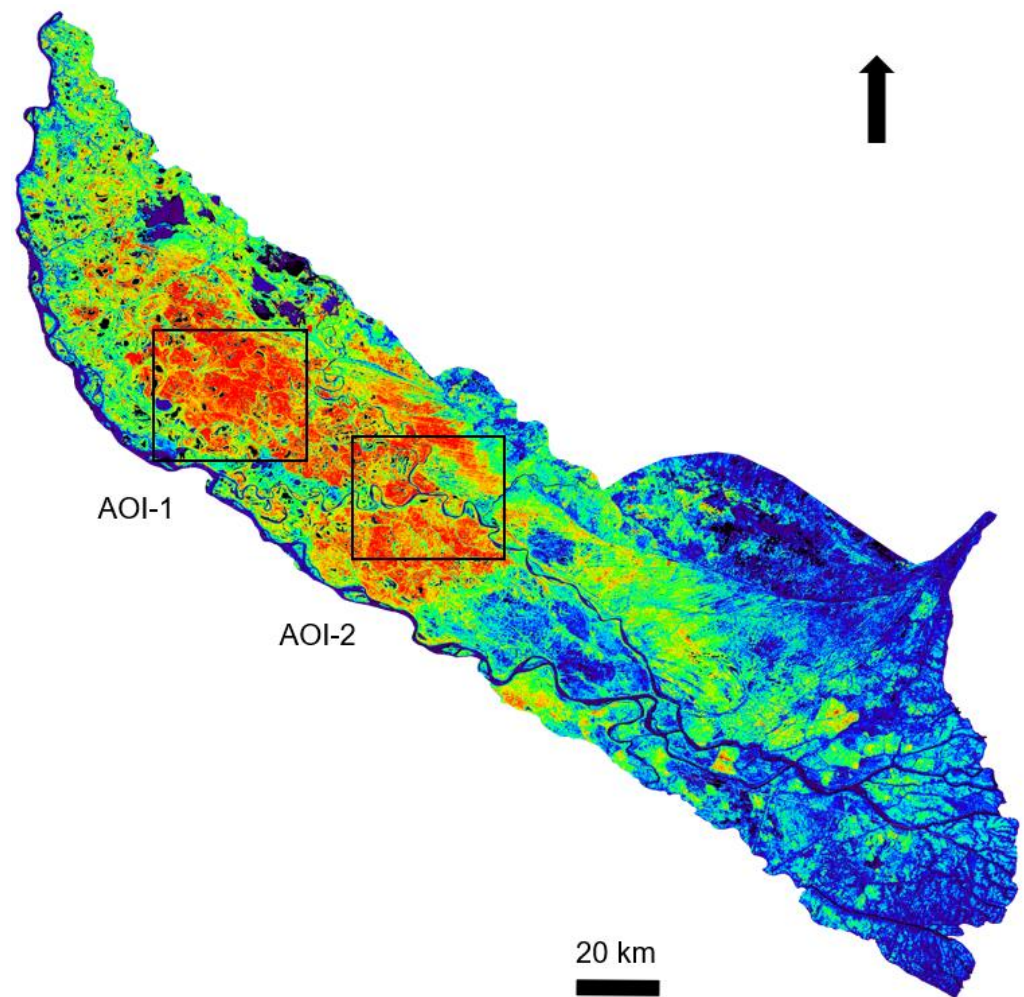
We use both the VV and VH polarizations to assess the capability of S1, using single and multirate averaged pre-fire and post-fire scenes to the performed mosaics and AOs, at 60-m and 10-m pixel resolutions, respectively.

Figure 8A,B shows a false-color composite optical (S2) and radar (S1) with S2-B12 (red), S2-B8 (green), and S1-HV (blue) for the Q1 (Figure 8A); S2-B12 (red), S2-B8 (green), and S1-HV (blue) for Q3 (Figure 8B). We use S1 as the master product, as its geolocation accuracy is high, after Range Doppler Terrain Correction, and we use the S2 as the slave product. Such combinations reveal patterns that are not clearly shown, using only optical data. The shades of blue given by the VH polarization (moderate- and high-vegetated cover) are more evident in Q1 than in Q3, demonstrating the evidence of the volume scattering by the total biomass available to be burned.



**Figure 8.** (A,B) False-color composite optical (S2) and radar (S1). (A). Quarter 1: RGB S2-B12 (red), S2-B8 (green), and S1-HV (blue). (B). Quarter 3: RGB S2-B12 (red), S2-B8 (green), and S1-HV (blue).

To discriminate the burnt affected area, from the fire unaffected areas, without using fixed thresholds, unsupervised and supervised classification were applied to the change detection algorithm (VV-VH), at a 60-m resolution. As shown in Figure 9 the burnt-affected area exhibits a strong patch homogenization that is clear (red-orange colors) in a visual comparison between the burned and unburned areas. From twenty initial classes, eight were selected, and, in this first stage, we considered all pixels affected by fire as high severity (red color) to moderate severity (orange color). The burned area classification with S1 (BAC S1) was validated with successive S2 mosaics from January, July, August, and September 2020, with a spatial resolution of 10-m. The overall accuracy and Kappa coefficient of the extracted results reached 74% and 0.43, respectively (Table 4). The results were the same as those obtained with the S2 (NBR 2), although commission errors persist.



**Figure 9.** Burned areas detection and mapping in the Paraná River Delta using S1 (change detection algorithm). The black box indicates the area of interest (AOI).

**Table 4.** Accuracy assessment of the Paraná River Delta burned area classification with S1(BAC S1).

		BAC S1		Total	Commission Errors
		Burned	Not-Burned		
S2-mosaic pixel 10-m	Burned	45	31	76	0.408
	Unburned	21	103	124	0.169
Total		66	134	200	
Omission errors		0.318	0.231		0.74

Overall accuracy: 74%. Kappa: 0.43.



SAR data at 10-m resolution shows a substantial difference, when comparing the pre-fire (Figure 10A,B) and post-fire (Figure 10C,D) images. The different colors visible in the C-band RGB composite, indicate the variations of fire disturbances. The purple-blue region, in Figure 10C displays a low backscatter at both the co- and cross-polarization, and correspond to a smooth burned area.

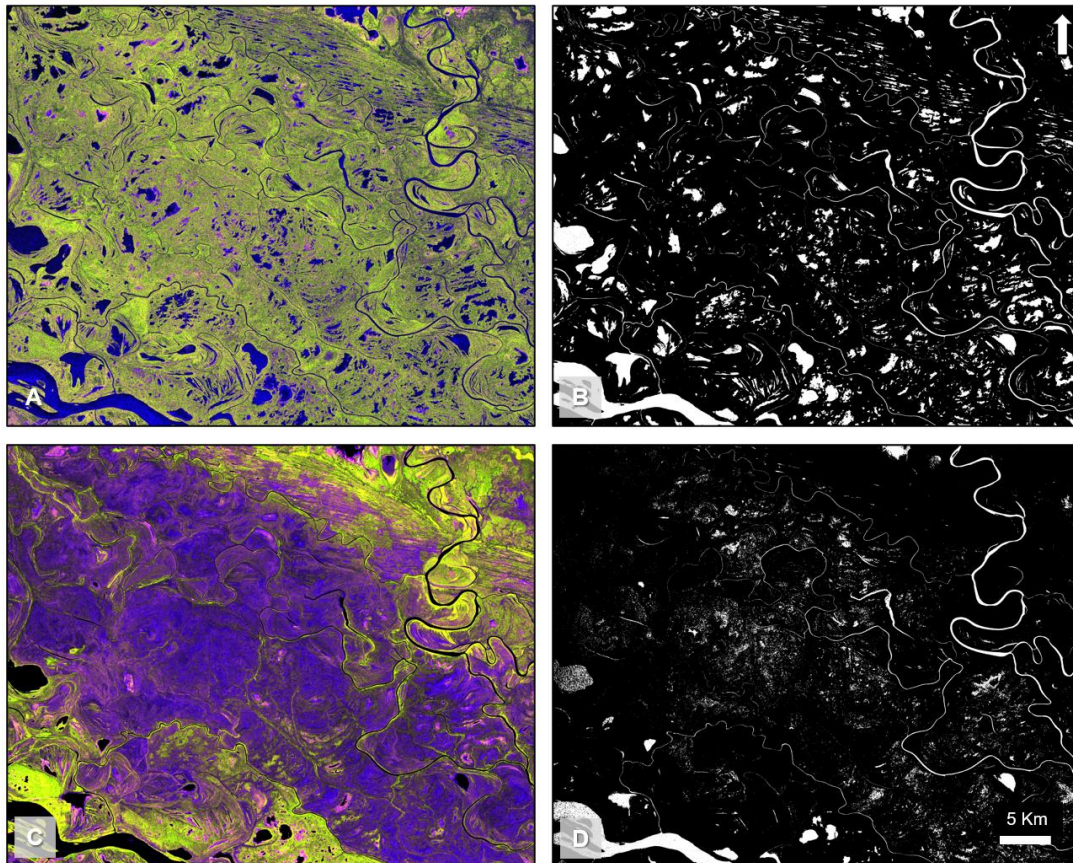


**Figure 10.** (A–D) AOI-1. (A). S1, average backscatter from January 2020 (Pre-fire), RGB CVV-CVH-ratio. (B). Water mask, January 2020 (Pre-fire). (C). S1, average backscatter from Quarter 3, 2020 (Post-fire), RGB CVV-CVH-ratio. (D). Water mask, Quarter 3, 2020 (Post-fire).

The difference in visualization corresponds to the superimposed monthly images of fire-AOIs during July, August, and September 2020 (Figure 11A–C). The burnt areas continued its expansion during this observation period. Figure 11D–F shows the trend in the RBRVH in decibels (dB) with a fire severity under dry environmental conditions. The volume dominated VH polarization, explains the increasing post-fire RBR with fire severity [40,44]. The RBR makes more distinguishable the burned areas, compared to all the other targets, exhibiting a higher contrast between the changed and unchanged surfaces. All pixels affected by fire are characterized by different severities with an increasing level from blue, cyan, green, yellow, orange, and red.

The AOI-2 (Figures 12A–D and 13A–F) show a similar behavior of the previously analyzed variables. These AOIs (1 and 2) represented the most heavily burned areas in the Paraná River Delta.

Fire reduces the scattering volume and, depending on its severity, would affect how much soil contributes to the backscatter signal. At the C-band (Figure 14A), fire is tough to detect, unless larger patches of grass and shrubs are burned (blue-purple colors). Fire events have an increased visibility at the L-band (Figure 14B), where stronger soil contributions enhance the double-bounce and hence brighten the backscatter signal [10,59].



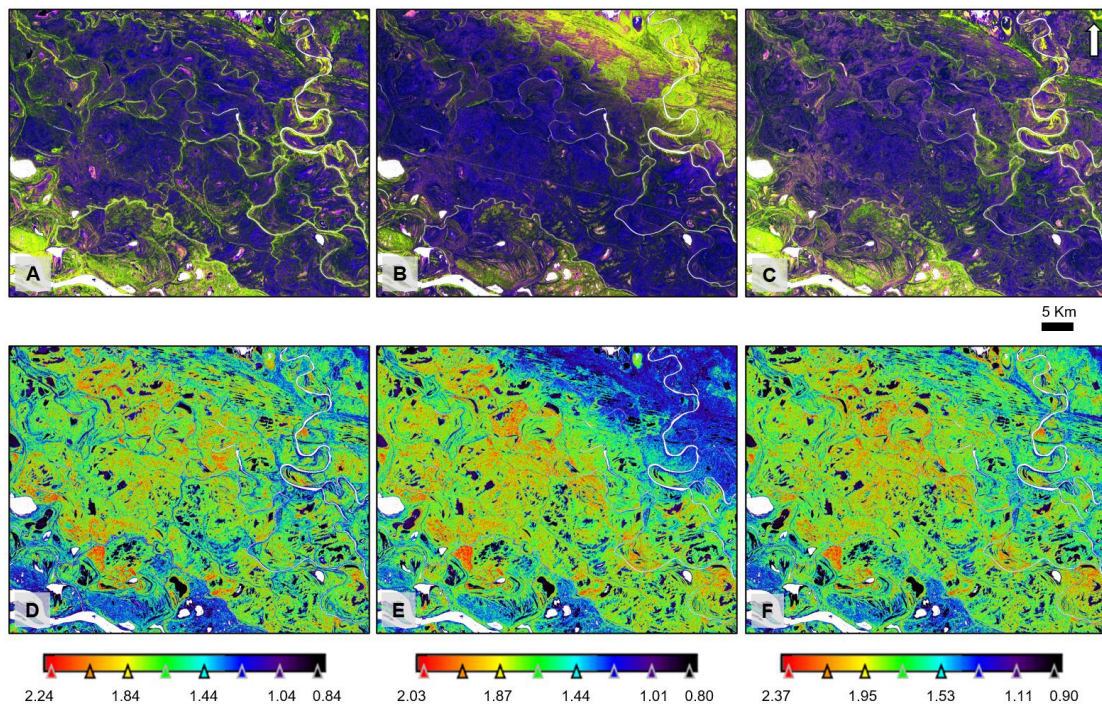


**Figure 11.** (A–F) AOI-1. (A–C). S1, average backscatter from July, August, and September 2020, respectively (Post-fire), RGB CVV-CVH-ratio. (D–F). Results for the radar burn ratio (RBRVH) from July, August, and September 2020, respectively, in decibels (dB).

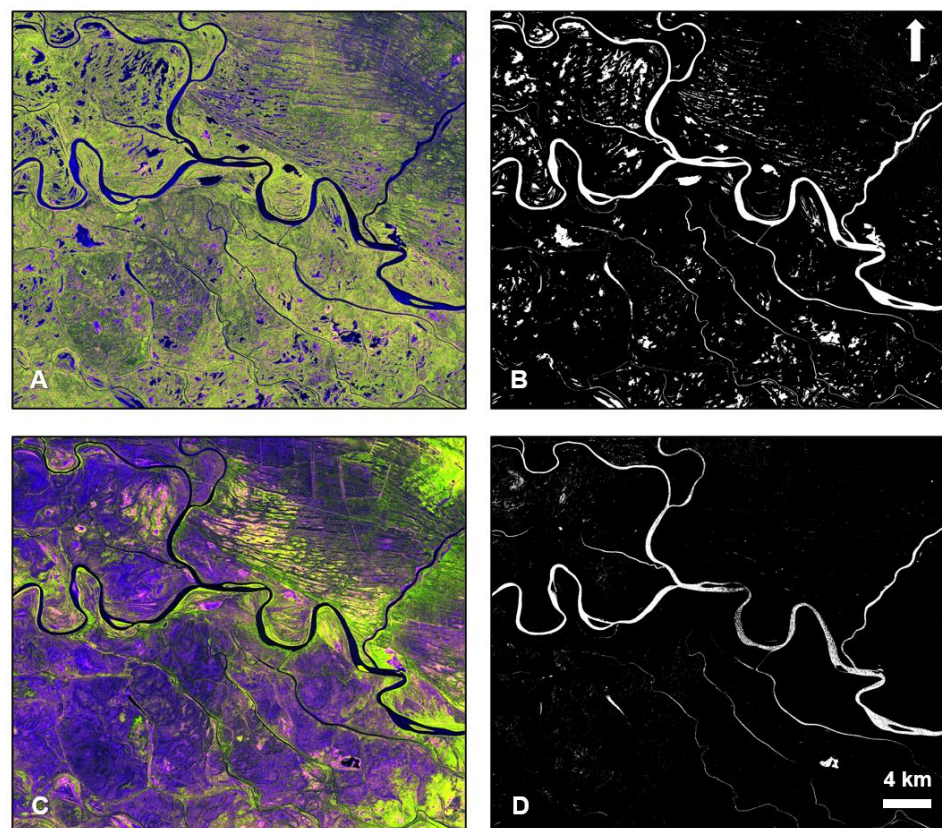


**Figure 12.** (A–D) AOI-2. (A). S1, average backscatter from January 2020 (Pre-fire), RGB CVV-CVH-ratio. (B). Water mask, January 2020 (Pre-fire). (C). S1, average backscatter from Quarter 3, 2020 (Post-fire), RGB CVV-CVH-ratio. (D). Water mask, Quarter 3, 2020 (Post-fire).



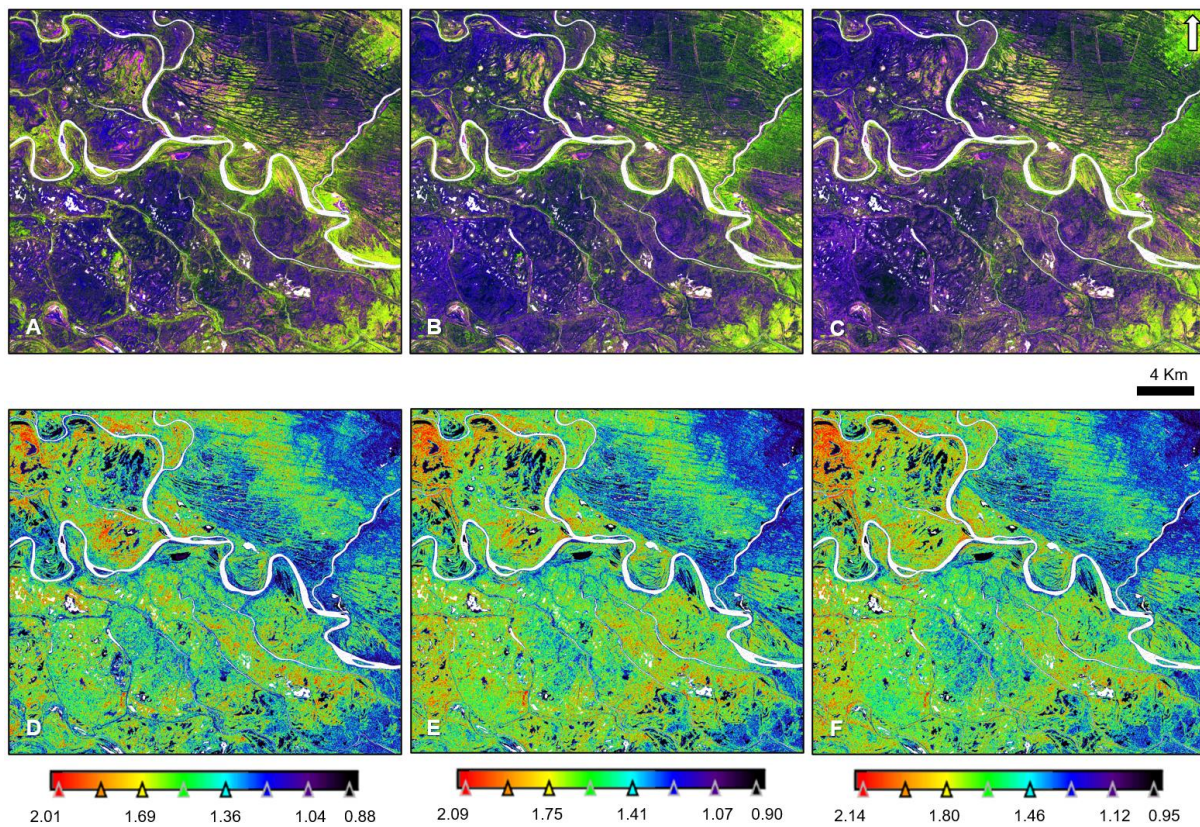


**Figure 13.** (A–F) AOI-2. (A–C). S1, average backscatter from July, August, and September 2020, respectively (Post-fire). RGB CVV-CVH-ratio. (D–F). Results for the radar burn ratio (RBRVH) from July, August, and September 2020, respectively, in decibels (dB).

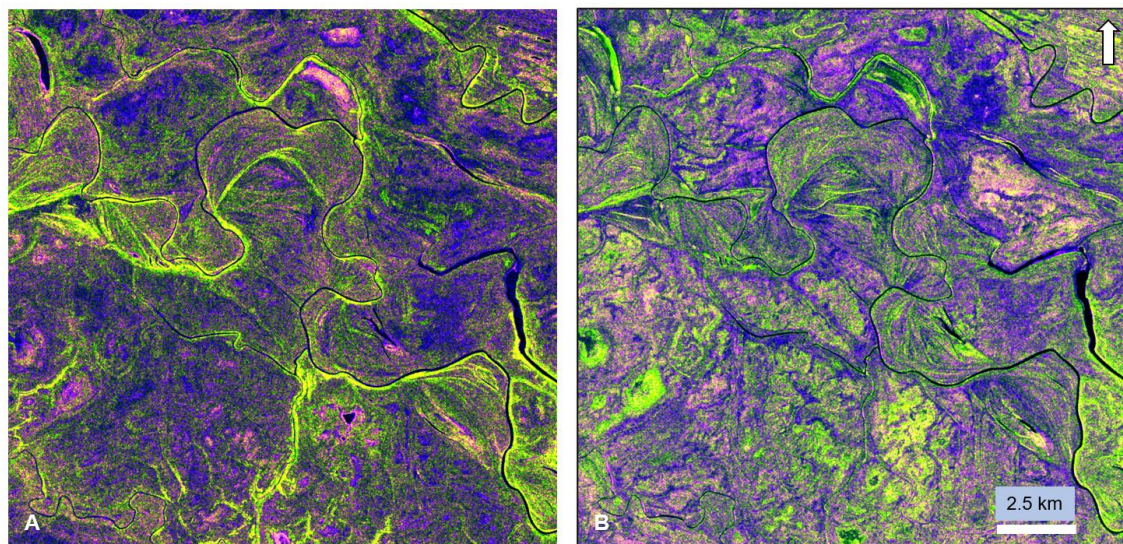


**Figure 14.** (A,B) (A). S1 subset from 28 July 2020. RGB CVV-CVH-ratio. (B). SAO1A SQP subset from 5 July 2020. RGB LHH-LHV-ratio. Pixel 10-m resolution.

CVH and LHV backscatters (green color) are closely correlated with unburned grasses, shrubs, and above-ground biomass, with LHV reaching higher  $\gamma_0$  values. Over time, as volume starts to be significantly degraded by the fire, the SAR signal follows a pattern of backscatter decrease in the burned areas. However, the severity of fire also determines the scattering mechanisms. In these examples, it is remarkable that both ratios and false-color



SAR composites, over this partially burned landscape, exhibit a similar appearance of dark blue-purple colors in the burned areas.

Both S1 and SQP images show differences in the burned area features that could indicate temporary flooded conditions. The C-band data also seem less useful than the L-band data in identifying burned areas.

Figure 15 shows the Pauli decomposition [60] for a TNQP SAO1A image, where the fire scars can be detected. The Pauli RGB color composite is based on a vector representation of linear combinations of scattering matrix elements. The resulting polarimetric channels are associated with red (double-bounce), green (volume scattering), and blue (single bounce or surface scattering). The burned areas appear dark blue (scattering over a surface) and patches of shades of red (corner reflector or double-bounce), where the different geophysical parameters of the ground, such as its humidity or roughness, are significantly altered.

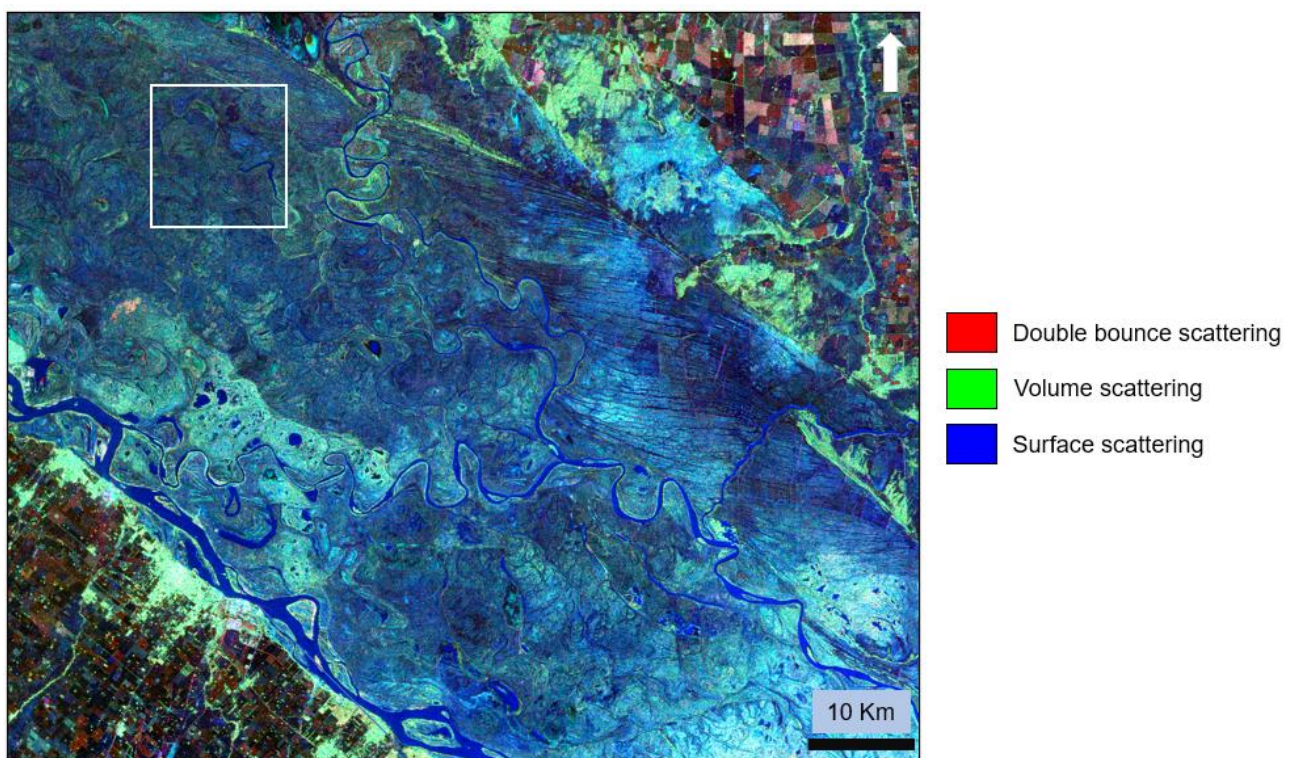


**Figure 15.** SAO1A subsets. Pauli color coding from the TOPSAR narrow quad polarization, descending right orbit, pixel 60-m, October 2020. White polygon locates Figure 14.

#### 4. Concluding Remarks

Applying radar and optical data integration to the evaluation and monitoring of land degradation, is far from being a uniform standardized process.

The spatial scale required for the Paraná River Delta is a critical issue as this wetland is highly heterogeneous, dissected, and is presented as an important challenge for the products here evaluated. The relationship between the landforms, vegetation cover, and the spatial and temporal resolutions imposed by the flood pulse, play a vital role in the quality of the results. Even so, the results obtained here are promising for post-flood and post-fire evaluation. Understanding the wetland environment, its hydrological pulse regime, its influence in vegetation patterns, and landscape configuration, is an important issue to improve the accuracy of the burned areas cartography; part of this can be better achieved by increasing the periodicity of the compositions of images between two weeks and a month.

The generation of water masks, through radar images, can contribute to improve the calculations of wetland burned areas, since it allows for the previous extraction of water surfaces that can confuse the burned area indices. Areas with fluctuating hydrological levels

leave dark soils with high contents of organic matter, which can be incorrectly classified as burned areas, due to their similar response to charcoal.

SAR and optical data integration can be certainly applied by other researchers or even wetlands managers, since S1, PAL1, L8, and S2 images are freely available and can also be processed in free open software, such as QGIS, SNAP, SAGA GIS, SARbian OS, and PolSARpro.

**Author Contributions:** Conceptualization, H.D.V. and P.G.A.; methodology, H.D.V. and W.F.S.; formal analysis, H.D.V.; writing H.D.V. and P.G.A.; review and editing P.G.A. and W.F.S. All authors have read and agreed to the published version of the manuscript.

**Funding:** This research received no external funding.

**Institutional Review Board Statement:** Not applicable.

**Informed Consent Statement:** Not applicable.

**Data Availability Statement:** Not applicable.

**Acknowledgments:** We want to thank all of the developers of the open-source software, as well as all the Space Agencies (ESA, NASA, CONAE) that offer free satellite imagery, which guarantees the basis of sustainable management of land use, with the prerequisite of broader knowledge and the gathering of expertise at different scales. We are also grateful for the technical support from the Universidad Autónoma de Entre Ríos (UADER), and CONICET PUE 56, Argentina.

**Conflicts of Interest:** The authors declare no conflict of interest.

## References

- Berkes, F.; Colding, J.; Folke, C. *Navigating Social-Ecological Systems: Building Resilience for Complexity and Change*; Cambridge University Press: Cambridge, UK, 2003; p. 393.
- Briassoulis, H. The socio-ecological fit of human responses to environmental degradation: An integrated assessment methodology. *Environ. Manag.* **2015**, *56*, 1448–1466. [[CrossRef](#)] [[PubMed](#)]
- Egidi, G.; Salvati, L.; Cudlin, P.; Salvia, R.; Romagnoli, M. A New ‘Lexicon’ of Land Degradation: Toward a Holistic Thinking for Complex Socioeconomic Issues. *Sustainability* **2020**, *12*, 4285. [[CrossRef](#)]
- Metternicht, G.; Zinck, J.A.; Blanco, P.D.; del Valle, H.F. Remote Sensing of Land Degradation: Experiences from Latin America and the Caribbean. *J. Environ. Qual.* **2010**, *39*, 42–61. [[CrossRef](#)] [[PubMed](#)]
- Dubovyk, O. The role of Remote Sensing in land degradation assessments: Opportunities and challenges. *Eur. J. Remote Sens.* **2017**, *50*, 601–613. [[CrossRef](#)]
- Del Valle, H.F.; Blanco, P.D.; Hardtke, L.A.; Metternicht, G.; Bouza, P.J.; Bisigato, A.; Rostagno, C.M. Contribution of Open Access Global SAR Mosaics to Soil Survey Programs at Regional Level: A Case Study in North-Eastern Patagonia. In *Geopedology: An Integration of Geomorphology and Pedology for Soil and Landscape Studies*; Zinck, J.A., Metternicht, G., Bocco, G., Del Valle, H.F., Eds.; Springer: New York, NY, USA, 2016; pp. 321–346.
- Joshi, N.; Baumann, M.; Ehammer, A.; Fensholt, R.; Grogan, K.; Hostert, P.; Jepsen, M.R.; Kuemmerle, T.; Meyfroidt, P.; Mitchard, E.T.A.; et al. A Review of the Application of Optical and Radar Remote Sensing Data Fusion to Land Use Mapping and Monitoring. *Remote Sens.* **2016**, *8*, 70. [[CrossRef](#)]
- Giuliani, G.; Chatenoux, B.; Piller, T.; Moser, F.; Lacroix, P. Data Cube on Demand (DCoD): Generating an earth observation Data Cube anywhere in the world. *Int. J. Appl. Earth Obs. Geoinf.* **2019**, *87*, 102035. [[CrossRef](#)]
- Rocchini, D.; Petras, V.; Petrasova, A.; Horning, N.; Furtkevicova, L.; Neteler, M.; Leutner, B.; Wegmann, M. Open data and open source for remote sensing training in ecology. *Ecol. Inform.* **2017**, *40*, 57–61. [[CrossRef](#)]
- Stefanidis, S.; Alexandridis, V.; Mallinis, G. A cloud-based mapping approach for assessing spatiotemporal changes in erosion dynamics due to biotic and abiotic disturbances in a Mediterranean Peri-Urban forest. *CATENA* **2022**, *218*. [[CrossRef](#)]
- Gemitzi, A.; Koutsias, N. A Google Earth Engine code to estimate properties of vegetation phenology in fire affected areas—A case study in North Evia wildfire event on August 2021. *Remote Sens. Appl. Soc. Environ.* **2022**, *26*, 100720. [[CrossRef](#)]
- Stefanidis, S.; Alexandridis, V.; Spalevic, V.; Mincato, R.L. Wildfire Effects on Soil Erosion Dynamics: The Case of 2021 Megafires in Greece. *J. Agric. For.* **2022**, *68*, 49–63.
- Silvestro, R.; Saulino, L.; Cavallo, C.; Allevato, E.; Pindozi, S.; Cervelli, E.; Conti, P.; Mazzoleni, S.; Saracino, A. The Footprint of Wildfires on Mediterranean Forest Ecosystem Services in Vesuvius National Park. *Fire* **2021**, *4*, 95. [[CrossRef](#)]
- Kalesnik, F.; Aceñolaza, P.G. Regional distribution of native and exotic species in levees of the lower delta of the Paraná River. *Acta Sci. Biol. Sci.* **2008**, *30*, 391–402. [[CrossRef](#)]

15. Kalesnik, F.; Vicari, R.; Aceñolaza, P.; Sirolli, H.; Bonan, L.; Iribarren, L.; Ramello, M.; Valle, J.; Bó, R. Restauración ecológica en humedales. Conservación y desarrollo sustentable en el Delta del Paraná. In *SIACRE-2015: Aportes y Conclusiones. Tomando Decisiones para Revertir la Degradación Ambiental*; Zuleta, G.A., Rovere, A.E., Mollard, F.P., Eds.; Vázquez Mazzini Editores: Buenos Aires, Argentina, 2017; Volume 22, pp. 193–202. (In Spanish)
16. Bedendo, D.J. Soils of Entre Rios. In *Soils of Argentina*; Rubio, G., Lavado, R.S., Pereyra, F.X., Eds.; Springer: Cham, Switzerland, 2019; pp. 165–173.
17. Neiff, J.; Mendiondo, M.; Depettris, C. ENSO Floods on River Ecosystems: Catastrophes or Myths? In *River Flood Defence (Kassel Reports of Hydraulic Engineering)*; Toenmsnann, F., Koch, M., Eds.; Herkules Verlag: Kassel, Germany, 2000; Volume 9, pp. 141–152.
18. Marchetti, Z.Y.; Aceñolaza, P.G. Evaluation of the relationships between floristic heterogeneity of *Panicum prionitis* Ness tall grasslands and the fire history, hydrological regime and soil texture in the Paraná River floodplain, Argentina. *Interciencia* **2011**, *36*, 600–607.
19. Salvia, M.; Franco, M.; Grings, F.; Perna, P.; Martino, R.; Karszenbaum, H.; Ferrazzoli, P. Estimating Flow Resistance of Wetlands Using SAR Images and Interaction Models. *Remote Sens.* **2009**, *1*, 992–1008. [[CrossRef](#)]
20. Zamboni, L.P.; Tentor, F.R.; Sione, W.F.; Hardtke, L.A.; del Valle, H.F.; Quignard, I.; Aceñolaza, P.G. Ecología del fuego en el Complejo Litoral del Río Paraná: Estimación de la ocurrencia de incendios a partir de mapas de focos de calor. *Interciencia* **2013**, *38*, 634–641. (In Spanish)
21. Marchetti, Z.Y.; Aceñolaza, P.G. Vegetation communities and their relationship with the pulse regime on islands of the Middle Paraná River, Argentina. *Iheringia Ser. Bot.* **2011**, *66*, 209–226.
22. Kandus, P.; Quintana, R.D. The Paraná River Delta. In *The Wetland Book*; Finlayson, C.M., Milton, G., Prentice, R., Davidson, N.C., Eds.; Springer: Dordrecht, The Netherlands, 2016; pp. 1–9.
23. Sione, W.; Aceñolaza, P.G.; Zamboni, L.P.; del Valle, H.F.; Serafini, C.; Gallardo Lancho, J.F. Estimación indirecta de emisiones de CO<sub>2</sub> a partir de información satelital en áreas quemadas de ambientes insulares del delta del río Paraná (Argentina). In *Emisiones de Gases con efecto Invernadero en ecosistemas Iberoamericanos*; Gallardo, J.F., Campo, J., Conti, M.E., Eds.; Editorial SiFyQA: Salamanca, Spain, 2009; pp. 255–272. (In Spanish)
24. Ipiña, A.; Salum, G.; Crinó, E.; Piacentini, R. Satellite and ground detection of very dense smoke clouds produced on the islands of the Paraná river delta that affected a large region in Central Argentina. *Adv. Space Res.* **2012**, *49*, 966–977. [[CrossRef](#)]
25. Grimm, A.M.; Almeida, A.S.; Beneti, C.A.A.; Leite, E.A. The combined effect of climate oscillations in producing extremes: The 2020 drought in southern Brazil. *RBRH* **2020**, *25*, e48. [[CrossRef](#)]
26. Ministerio de Ambiente y Desarrollo Sostenible. *Informe de superficies afectadas por incendios en el Delta e islas del Río Paraná Enero-Septiembre 2020*; Dirección Nacional de Planificación y Ordenamiento Ambiental del Territorio: Buenos Aires, Argentina, 2020; p. 40. (In Spanish)
27. Aceñolaza, P.; Zamboni, L.; Sione, W.; Kalesnik, F. Caracterización de la región superior del Complejo litoral del Río Paraná: Grandes Unidades de ambiente. *Ser. Miscelánea INSUGEO* **2008**, *17*, 293–308. (In Spanish)
28. Sica, Y.V.; Quintana, R.D.; Radeloff, V.C.; Gavier-Pizarro, G.I. Wetland loss due to land-use change in the Lower Paraná River Delta, Argentina. *Sci. Total Environ.* **2016**, *568*, 967–978. [[CrossRef](#)]
29. Aquino, D.S.; Gavier-Pizarro, G.; Quintana, R.D. Disentangling the effects of hydro-climatic factors and land use intensification on wetland vegetation dynamics in the Lower Delta of the Paraná River. *Remote Sens. Appl. Soc. Environ.* **2021**, *21*, 100466. [[CrossRef](#)]
30. Salvia, M.; Ceballos, D.; Grings, F.; Karszenbaum, H.; Kandus, P. Post-Fire Effects in Wetland Environments: Landscape Assessment of Plant Coverage and Soil Recovery in the Paraná River Delta Marshes, Argentina. *Fire Ecol.* **2012**, *8*, 17–37. [[CrossRef](#)]
31. Kandus, P.; Quintana, R.D.; Minotti, P.G.; Oddi, P.D.J.; Baigún, C.; González Trilla, G.; Ceballos, D.S. Ecosistemas de humedal y una perspectiva hidrogeomórfica como marco para la valoración ecológica de sus bienes y servicios. In *Valoración de Servicios Ecosistémicos. Conceptos, Herramientas y Aplicaciones para el Ordenamiento Territorial*; Littera, P., Jobbágy, E.G., Paruelo, J.M., Eds.; Ediciones INTA: Buenos Aires, Argentina, 2011; pp. 265–290. (In Spanish)
32. Minotti, P. The Paraná-Paraguay Fluvial Corridor (Argentina). In *The Wetland Book*, Finlayson, C.M.; Milton, G., Prentice, R., Davidson, N.C., Eds.; Springer: Dordrecht, The Netherlands, 2018; pp. 785–796. [[CrossRef](#)]
33. CONAE. SAOCOM-1 Level 1 Product Format. SAOCOM Project. 13 January 2020. Available online: [https://catalogos.conae.gov.ar/catalogo/docs/SAOCOM/SAOCOM-1\\_SAR\\_Level-1\\_Product-Format\\_13Jan2020.pdf](https://catalogos.conae.gov.ar/catalogo/docs/SAOCOM/SAOCOM-1_SAR_Level-1_Product-Format_13Jan2020.pdf) (accessed on 15 December 2020).
34. Kirches, G. Algorithm Theoretical Basis Document Sentinel 2 Global Mosaics Copernicus Sentinel-2 Global Mosaic (S2GM) within the Global Land Component of the Copernicus Land Service. Available online: [https://usermanual.readthedocs.io/en/1.1.2/\\_downloads/5a2d961d53dea1eb1117ec73e4cbff09/S2GM-SC2-ATBD-BC-v1.3.2.pdf](https://usermanual.readthedocs.io/en/1.1.2/_downloads/5a2d961d53dea1eb1117ec73e4cbff09/S2GM-SC2-ATBD-BC-v1.3.2.pdf) (accessed on 15 December 2020).
35. QGIS Development Team. QGIS Geographic Information System. Open Credit Geospatial Foundation. Available online: <http://qgis.osgeo.org> (accessed on 15 January 2020).
36. Conrad, O.; Bechtel, B.; Bock, M.; Dietrich, H.; Fischer, E.; Gerlitz, L.; Wehberg, J.; Wichmann, V.; Böhner, J. System for Automated Geoscientific Analyses (SAGA) v. 2.1.4. *Geosci. Model Dev.* **2015**, *8*, 1991–2007. [[CrossRef](#)]
37. SAS Planet Development Team. SAS. Planet v180518.9750 Nightly. Available online: <http://sasgis.org/> (accessed on 15 December 2020).
38. Scientific Exploitation of Operational Missions. Sentinel Application Platform (SNAP). Scientific Exploitation of Operational Missions, European Spatial Agency. Available online: <https://www.eoportal.org/other-space-activities/snap-sentinel-application-platform#snap-sentinel-application-platform-toolbox> (accessed on 10 January 2022).



39. Google, LLC. Available online: <https://www.google.com/> (accessed on 21 July 2020).
40. R Core Team. *R: A Language and Environment for Statistical Computing*; R Foundation for Statistical Computing; Available online: <https://www.R-project.org/> (accessed on 10 January 2022).
41. Miller, J.D.; Thode, A.E. Quantifying burn severity in a heterogeneous landscape with a relative version of the delta Normalized Burn Ratio (dNBR). *Remote Sens. Environ.* **2007**, *109*, 66–80. [[CrossRef](#)]
42. Stroppiana, D.; Bordogna, G.; Carrara, P.; Boschetti, M.; Boschetti, L.; Brivio, P.A. A method for extracting burned areas from Landsat TM/ETM+ images by soft aggregation of multiple Spectral Indices and a region growing algorithm. *ISPRS J. Photogramm. Remote Sens.* **2012**, *69*, 88–102. [[CrossRef](#)]
43. Giglio, L.; Boschetti, L.; Roy, D.P.; Humber, M.L.; Justice, C.O. The Collection 6 MODIS burned area mapping algorithm and product. *Remote Sens. Environ.* **2018**, *217*, 72–85. [[CrossRef](#)]
44. Tanase, M.; Kennedy, R.; Aponte, C. Radar Burn Ratio for fire severity estimation at canopy level: An example for temperate forests. *Remote Sens. Environ.* **2015**, *170*, 14–31. [[CrossRef](#)]
45. Durante, M.; Di Bella, C.M. A MODIS based tool to assess inundation patterns: An example for the Paraná Delta River. *RIA* **2020**, *46*, 30–45.
46. Pleniou, M.; Koutsias, N. Sensitivity of spectral reflectance values to different burn and vegetation ratios: A multi-scale approach applied in a fire-affected area. *ISPRS J. Photogramm. Remote Sens.* **2013**, *79*, 199–210. [[CrossRef](#)]
47. Lanorte, A.; Danese, M.; Lasaponara, R.; Murgante, B. Multiscale mapping of burn area and severity using multisensor satellite data and spatial autocorrelation analysis. *Int. J. Appl. Earth Observ. Geoinf.* **2013**, *20*, 42–51. [[CrossRef](#)]
48. Lasaponara, R.; Tucci, B. Identification of Burned Areas and Severity Using SAR Sentinel-1. *IEEE Geosci. Remote Sens. Lett.* **2019**, *16*, 917–921. [[CrossRef](#)]
49. Kalogirou, V.; Ferrazzoli, P.; Vecchia, A.D.; Fomelis, M. On the SAR backscatter of burned forest: A model-based study in C-band, over burned pine canopies. *IEEE Trans. Geosci. Remote Sens.* **2004**, *52*, 6205–6215. [[CrossRef](#)]
50. Imperatore, P.; Azar, R.; Calo, F.; Stroppiana, D.; Brivio, P.A.; Lanari, R.; Pepe, A. Effect of the Vegetation Fire on Backscattering: An Investigation Based on Sentinel-1 Observations. *IEEE J. Sel. Top. Appl. Earth Obs. Remote Sens.* **2017**, *10*, 4478–4492. [[CrossRef](#)]
51. Szpakowski, D.M.; Jensen, J.L.R. A Review of the Applications of Remote Sensing in Fire Ecology. *Remote Sens.* **2019**, *11*, 2638. [[CrossRef](#)]
52. Tanase, M.A.; Belenguer-Plomer, M.A.; Roteta, E.; Bastarrika, A.; Wheeler, J.; Fernández-Carrillo, Á.; Tansey, K.; Wiedemann, W.; Navratil, P.; Lohberger, S.; et al. Burned Area Detection and Mapping: Intercomparison of Sentinel-1 and Sentinel-2 Based Algorithms over Tropical Africa. *Remote Sens.* **2020**, *12*, 334. [[CrossRef](#)]
53. Verhegghen, A.; Eva, H.; Ceccherini, G.; Achard, F.; Gond, V.; Gourlet-Fleury, S.; Cerutti, P.O. The Potential of Sentinel Satellites for Burnt Area Mapping and Monitoring in the Congo Basin Forests. *Remote Sens.* **2016**, *8*, 986. [[CrossRef](#)]
54. Belenguer-Plomer, M.A.; Tanase, M.A.; Fernandez-Carrillo, A.; Chuvieco, E. Burned area detection and mapping using sentinel-1 backscatter coefficient and thermal anomalies. *Remote Sens. Environ.* **2019**, *233*, 111345. [[CrossRef](#)]
55. Puig, A.; Salinas, H.F.O.; Borús, J.A. Relevance of the Paraná River hydrology on the fluvial water quality of the Delta Biosphere Reserve. *Environ. Sci. Pollut. Res.* **2015**, *23*, 11430–11447. [[CrossRef](#)]
56. Li, X.; Song, K.; Liu, G. Wetland Fire Scar Monitoring and Its Response to Changes of the Pantanal Wetland. *Sensors* **2020**, *20*, 4268. [[CrossRef](#)]
57. Zamboni, L.P.; Aceñolaza, P.G. Efectos del Fuego sobre la biomasa vegetal en un área del Predelta del río Paraná. (Entre Ríos, Argentina). *Boletín De La Soc. Argent. De Botánica* **2005**, *40*, 90. (In Spanish)
58. Bixby, R.J.; Cooper, S.D.; Gresswell, R.E.; Brown, L.E.; Dahm, C.N.; Dwire, K.A. Fire effects on aquatic ecosystems: An assessment of the current state of the science. *Freshw. Sci.* **2015**, *34*, 1340–1350. [[CrossRef](#)]
59. Kellndorfer, J. Using SAR data for mapping deforestation and forest degradation. In *The SAR Handbook: Comprehensive Methodologies for Forest Monitoring and Biomass Estimation*; Flores, A., Herndon, K., Thapa, R., Cherrington, E., Eds.; Servir Global: Washington, DC, USA, 2019; pp. 65–172. [[CrossRef](#)]
60. Lee, J.S.; Pottier, E. *Polarimetric Radar Imaging: From Basics to Applications*; CRC Press: Boca Raton, FL, USA, 2009; p. 422.